Journal of Controlled Release 195 (2014) 63–71

Contents lists available at ScienceDirect

Journal of Controlled Release

journal homepage: www.elsevier.com/locate/jconrel

cRGD-directed, NIR-responsive and robust AuNR/PEG–PCL hybrid nanoparticles for targeted chemotherapy of glioblastoma *in vivo*

Yinan Zhong [a], Chao Wang [b], Ru Cheng [a], Liang Cheng [b], Fenghua Meng [a,*], Zhuang Liu [b,*], Zhiyuan Zhong [a,*]

[a] Biomedical Polymers Laboratory and Jiangsu Key Laboratory of Advanced Functional Polymer Design and Application, College of Chemistry, Chemical Engineering and Materials Science, Soochow University, Suzhou 215123, PR China
[b] Jiangsu Key Laboratory for Carbon-Based Functional Materials & Devices, Institute of Functional Nano & Soft Materials (FUNSOM), Soochow University, Suzhou 215123, PR China

ARTICLE INFO

Article history:
Received 19 May 2014
Accepted 29 July 2014
Available online 7 August 2014

Keywords:
cRGD
Gold nanorods
Biodegradable nanoparticles
Doxorubicin
NIR-sensitive
Glioblastoma

ABSTRACT

cRGD-directed, NIR-responsive and robust AuNR/PEG–PCL hybrid nanoparticles (cRGD-HNs) were designed and developed for targeted chemotherapy of human glioma xenografts in mice. As expected, cRGD-HNs had excellent colloidal stability. The *in vitro* release studies showed that drug release from DOX-loaded cRGD-HNs (cRGD-HN-DOX) was minimal under physiological conditions but markedly accelerated upon NIR irradiation at a low power density of 0.2 W/cm^2, due to photothermally induced phase transition of PCL regime. MTT assays showed that the antitumor activity of cRGD-HN-DOX in $\alpha_v\beta_3$ integrin over-expressed human glioblastoma U87MG cells was greatly boosted by mild NIR irradiation, which was significantly more potent than non-targeting HN-DOX counterpart under otherwise the same conditions and was comparable or superior to free DOX, supporting receptor-mediated endocytosis mechanism. The *in vivo* pharmacokinetics studies showed that cRGD-HN-DOX had much longer circulation time than free DOX. The *in vivo* imaging and biodistribution studies revealed that cRGD-HN-DOX could actively target human U87MG glioma xenograft in nude mice. The therapeutic studies in human U87MG glioma xenografts exhibited that cRGD-HN-DOX in combination with NIR irradiation completely inhibited tumor growth and possessed much lower side effects than free DOX. The Kaplan–Meier survival curves showed that all mice treated with cRGD-HN-DOX plus NIR irradiation survived over an experimental period of 48 days while control groups treated with PBS, cRGD-HN-DOX, cRGD-HNs with NIR irradiation, free DOX, or HN-DOX with NIR irradiation (non-targeting control) had short life spans of 15–40 days. Ligand-directed AuNR/PEG–PCL hybrid nanoparticles with evident tumor-targetability as well as superior spatiotemporal and rate control over drug release have emerged as an appealing platform for cancer chemotherapy *in vivo*.

1. Introduction

Biodegradable micelles based on amphiphilic block copolymers of poly(ethylene glycol) (PEG) and aliphatic polyesters such as poly(ε-caprolactone) (PCL), polylactide (PLA), and poly(lactide-co-glycolide) (PLGA) are among the most studied nanocarriers for targeted and controlled delivery of poorly water soluble chemotherapeutic agents including paclitaxel (PTX) and doxorubicin (DOX) [1–3]. It is interesting to note that a couple of micellar drugs such as Genexol-PM (PTX formulation based on PEG-*b*-PLA micelles) and BIND-014 (micellar docetaxel formulation based on PEG-PDLLA or PEG-PLGA targeting to prostate cancer) have been translated to the clinical trials [4,5]. The current micellar drugs are, however, often associated with problems of low *in vivo* stability, premature drug release, inefficient tumor cell uptake, as well as slow drug release in the tumor site and inside the tumor cells, which would not only greatly reduce their therapeutic efficacy but also induce systemic side effects [6–8].

In the past years, different strategies have been explored to improve the targetability and *in vivo* drug release behaviors of biodegradable micelles. For example, crosslinked micelles have been developed to achieve better *in vivo* stability and prolonged circulation time, thereby enhancing drug accumulation in the tumor site *via* the enhanced permeability and retention (EPR) effect [9,10]. In particular, stimuli-sensitive degradable crosslinked micelles that are de-crosslinked or hydrolyzed in response to the reducing environment in the cytosol or acidic pH in the endo/lysosomal compartments are of interest, as they not only possess enhanced stability but also trigger drug release inside the tumor cells [11–15]. Several groups reported that stimuli-sensitive degradable crosslinked micelles exhibit improved antitumor efficacy and reduced systemic toxicity *in vivo* as compared to the stimuli-insensitive or non-crosslinked controls [16–20]. It should be noted, however, that these sophisticated micelles are typically based on new functional block copolymers, which usually involve multi-step

* Corresponding authors. Tel./fax: +86 512 6588 0098.
E-mail addresses: fhmeng@suda.edu.cn (F. Meng), zliu@suda.edu.cn (Z. Liu), zyzhong@suda.edu.cn (Z. Zhong).

http://dx.doi.org/10.1016/j.jconrel.2014.07.054
0168-3659/

synthesis. Moreover, drug release from stimuli-sensitive crosslinked micelles inside the tumor cells is often slow and lacks control. Very recently, we reported that micelles prepared by coating gold nanorods (AuNRs) with PEG-*b*-PCL-lipoic acid ester (PEG–PCL–LA) block copolymer while possessing high stability exhibited excellent temporal, spatial and rate control over drug release via mild NIR irradiation, resulting in effective inhibition of both drug-sensitive and drug-resistant (acquired drug resistance, ADR) cancer cells [21]. Interestingly, Jerome et al. reported similar results almost at the same time [22]. Lipoic acid is a natural anti-oxidant that is produced by the human body [23,24]. Lipoic acid with a high affinity to gold surface has widely been used to stabilize gold nanoparticles in aqueous environment [25–28]. In our lab, based on ring-opening polymerizability of lipoic ring to form linear polydisulfide in the presence of catalytic amount of dithiothreitol, we have prepared reduction-sensitive reversibly crosslinked micelles and nanoparticles from various polymeric conjugates of lipoic acid [29–33].

In this paper, we report on cRGD-directed AuNR/PEG–PCL hybrid nanoparticles (cRGD-HNs) for targeted chemotherapy of glioblastoma in mice (Scheme 1). cRGD has a high affinity with the $\alpha_v\beta_3$ integrin receptors over-expressed on angiogenic endothelial cells as well as tumor cells such as malignant glioma cells, breast cancer cells, bladder cancer cells and prostate cancer cells, which render cRGD a unique molecular ligand for targeted cancer chemotherapy [34,35]. Several groups reported that cRGD-functionalized nanoparticles exhibited enhanced antitumor effects toward glioblastoma *in vitro* and *in vivo* as compared to the non-targeting counterpart [36–39]. Herein, cRGD-HNs were designed with the following features: (i) they have defined shape and size and are particularly robust in circulation minimizing premature drug release and improving *in vivo* pharmacokinetics, as AuNRs are covalently coated with a layer of PEG–PCL–LA copolymer; (ii) they can be recognized and taken up by glioblastoma cells via the receptor-mediated endocytosis mechanism; and (iii) drug release can be remotely controlled by NIR laser, which triggers drug release into tumor extracellular environment as well as inside the target tumor cells, resulting in enhanced tumor penetration and potent antitumor effect. Here, preparation of DOX-loaded cRGD-HNs (cRGD-HN-DOX), specificity and antitumor activity toward human glioblastoma U87MG cells, *in vivo* pharmacokinetics and biodistribution, as well as therapeutic effects in human glioblastoma xenografts in mice were investigated.

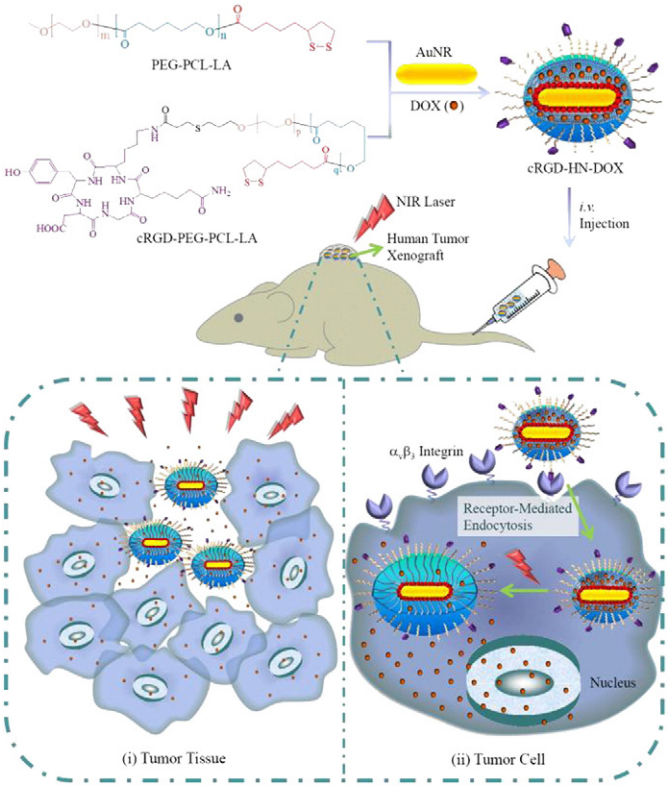

Scheme 1. Illustration of cRGD-directed and NIR-responsive AuNR/PEG-PCL hybrid nanoparticles (cRGD-HNs) for targeted delivery of DOX to human glioblastoma xenograft in mice. The release of drug is remotely controlled by NIR laser, wherein (i) for nanoparticles remaining in the tumor extracellular milieu, triggering drug release would enhance drug tumor penetration; and (ii) for nanoparticles taken up by cells via receptor-mediated endocytosis mechanism, fast intracellular drug release results in potent antitumor effect.

2. Materials and methods

2.1. Materials

Dichloromethane (DCM) was dried by refluxing over CaH_2 and distilled before use. Sodium borohydride ($NaBH_4$, Sigma), cetyltrimethyl ammonium bromide (CTAB, Sigma), ascorbic acid (Sigma), silver nitrate ($AgNO_3$, Sigma), tetrachloroauric acid ($HAuCl_4 \times 3H_2O$, Sigma), lipoic acid (98%, Acros), N, N-dicyclohexyl carbodiimide (DCC, 99%, Alfa Aesar), 4-(dimethylamino)pyridine (DMAP, 99%, Alfa Aesar), cRGD (98%, ChinaPeptides Co., Ltd.), 1-(3-dimethylaminopropyl)-3-ethylcarbodiimide hydrochloride (EDC·HCl, Adamas Reagent Co., Ltd.), N-hydroxysuccinimide (NHS, J&K), triethylamine (Et_3N, 99%, Alfa Aesar), dimethyl sulfoxide (DMSO), doxorubicin hydrochloride (DOX·HCl, 99%, Beijing ZhongShuo Pharmaceutical Technology Development Co., Ltd.), and Cy 7 (Beijing Fanbo biochemicals) were used as received. PEG-*b*-PCL-lipoic acid ester (PEG–PCL–LA) (M_n = 5.0–3.1 kg/mol, PDI = 1.08) and allyl-PEG-*b*-PCL (M_n = 7.8–3.0 kg/mol, PDI = 1.06) block copolymers, as well as lipoic acid anhydride were synthesized according to our previous reports [21,40,41]. AuNRs were prepared according to a reported method [42]. The concentration of AuNRs was determined by the absorbance at 808 nm with a molar extinction coefficient of $4.4 \pm 0.5 \times 10^9$ L · mol^{-1} cm^{-1} [43].

2.2. Synthesis of cRGD-PEG-b-PCL-LA block copolymer

cRGD-PEG-*b*-PCL-LA copolymer was prepared in three steps from allyl-PEG-*b*-PCL. Firstly, under a N_2 atmosphere, to a 25 mL reaction vessel equipped with a magnetic stirrer were introduced allyl-PEG-*b*-PCL (2.50 g, 0.231 mmol), mercaptopropionic acid (0.49 g, 4.63 mmol), AIBN (0.56 g, 3.46 mmol), and dry DMF (30 mL). The mixture was stirred at 70 °C for 24 h. The product, carboxyl-PEG-*b*-PCL, was isolated by precipitation in cold diethyl ether, washed several times with diethyl ether, and dried *in vacuo* at room temperature. Yield: 87%. Then, to a solution of carboxyl-PEG-*b*-PCL (2.0 g, 0.19 mmol) in DCM (15.0 mL) was added 4-(dimethylamino) pyridine (4.6 mg, 0.38 mmol) solution in DCM (1.0 mL) and lipoic acid anhydride (0.15 g, 0.38 mmol) in DCM (1.0 mL). The mixture was stirred for 48 h under N_2 at 30 °C. The product, carboxyl-PEG-*b*-PCL-LA, was isolated by precipitation in cold diethyl ether, washed several times with diethyl ether, and dried *in vacuo* at room temperature. Yield: 84%. M_n (GPC) = 21.0 kg/mol, PDI = 1.06. Finally, cRGD was conjugated to carboxyl-PEG-*b*-PCL-LA by carbodiimide chemistry. Carboxyl-PEG-*b*-PCL (1.0 g, 0.093 mmol) in 10 mL DMF was added to a solution of cRGD (70 mg, 0.12 mmol) in phosphate buffer (PB, 10 mM, pH 7.4) in the presence of EDC (53 mg, 0.28 mmol) and NHS (16 mg, 0.14 mmol). The reaction proceeded for 24 h at room temperature. The final product, cRGD-PEG-*b*-PCL-LA, was isolated through dialysis against deionized water for 48 h (MWCO 3500) followed by lyophilization. Yield: 77%. ^{1}H NMR (400 MHz, DMSO-d_6): PEG: δ 3.38, 3.63; PCL: δ 1.35, 1.65, 2.30, 4.10, 4.22; lipoic ring: δ 1.90, 3.22; cRGD moiety: δ 6.84–7.61. M_n (^{1}H NMR) = 10.8 kg/mol. The degree of cRGD conjugation was determined to be 45% by the Micro BCA Protein assay kit.

2.3. Characterization

^{1}H NMR spectra were recorded on a Unity Inova 400 spectrometer operating at 400 MHz using deuterated chloroform ($CDCl_3$) or deuterated dimethylsulfoxide (DMSO-d_6) as a solvent. The chemical shifts were calibrated against residual $CHCl_3$ or DMSO solvent signals. The molecular weight and polydispersity of the copolymers were determined by a Waters 1515 gel permeation chromatograph (GPC) instrument equipped with two linear PLgel columns (500 Å and Mixed-C) following a guard column and a differential refractive-index detector (RI 2414). The measurements were performed using THF as the eluent at a flow rate of 1.0 mL/min at 30 °C and a series of narrow polystyrene standards for the calibration of the columns. The size of micelles was determined using dynamic light scattering (DLS). Measurements were carried out at 25 °C using Zetasizer Nano-ZS from Malvern Instruments equipped with a 633 nm He–Ne laser using back-scattering detection. Transmission electron microscopy (TEM) was performed using a Tecnai G220 TEM operated at an accelerating voltage of 200 kV.

2.4. Preparation of cRGD-HNs

cRGD-directed AuNR/PEG–PCL hybrid nanoparticles (cRGD-HNs) were prepared by dropwise adding a cRGD-PEG-*b*-PCL-LA block copolymer solution (2.0 mL, 5.0 mg/mL) in DMF to an AuNRs dispersion (5.0 mL, 0.1 mg/mL) in deionized water under vigorous stirring. AuNRs were purified by centrifugation (Thermo Scientific MicroCL 21/21R) and washing (14.8 krpm, 12 min, twice) to remove excess CTAB coating molecules prior to the reaction. The reaction was allowed to proceed for 4 h under stirring. cRGD-HNs were collected by centrifugation and twice washing with water (14.8 krpm, 12 min), wherein excess free polymer if present would be removed.

2.5. Loading and NIR-triggered release of DOX

Loading of DOX into cRGD-HNs was accomplished by mixing a DOX solution in DMSO (5.0 mg/mL) with a cRGD-HNs solution (0.1 mg/mL) in PB (10 mM, pH 7.4). The mixture was stirred for 30 min and incubated at room temperature for 12 h. Free DOX was removed by extensive dialysis against PB for 24 h using a dialysis membrane (MWCO 3500) at room temperature. The whole procedure was performed in the dark. The obtained DOX-loaded cRGD-HNs (cRGD-HN-DOX) were stored under 4 °C in the dark.

To determine drug loading content (DLC), cRGD-HN-DOX samples were dissolved in hydrochloric acid–isopropanol (HCl–IPA) [44]. DOX was extracted from cRGD-HN-DOX by HCl–IPA, collected following centrifugation, and then analyzed using fluorescence measurement (FLS920, excitation at 480 nm, emission range from 500 nm to 650 nm). A calibration curve was obtained from DOX/HCl–IPA solutions with different given DOX concentrations. The amount of DOX was determined by fluorescence measurement. The DLC and drug loading efficiency (DLE) were determined according to the following formula:

DLC (*wt.*%) (weight of loaded drug/total weight of loaded drug and cRGD-HNs) × 100%

DLE (%) (weight of loaded drug/weight of drug in feed) × 100%.

NIR-triggered drug release was performed in PB (10 mM, pH 7.4) at 37 °C. An optical-fiber coupled power-tunable diode laser (continuous wave) with wavelengths at 808 nm (maximal power = 10 W, Hi-Tech Optoelectronics Co., Beijing, China) was employed. The laser beams were regulated to be a round shape with a diameter of 3.4 cm. cRGD-HN-DOX was dispersed in 10.0 mL PB (10 mM, pH 7.4) using a 15.0 mL test tube. At desired time intervals, the samples were irradiated with NIR laser at an output power of 0.2 W/cm^2 for 5 min and 500 μL of the resulting solutions was taken out for analysis. The amount of DOX released in the supernatant of release media following centrifugation at 14.8 krpm for 12 min were determined by fluorescence measurement.

2.6. In vitro cytotoxicity assays

Human glioblastoma U87MG cells were plated in a 96-well plate (5×10^4 cells/well) in 100 μL of low glucose Dulbecco's Modified Eagle medium (DMEM) supplemented with 10% fetal bovine serum, 1% L-glutamine, antibiotics penicillin (100 IU/mL), and streptomycin (100 μg/mL) for 12 h. 20 μL of cRGD-HN-DOX, HN-DOX, blank cRGD-HNs, HNs or free DOX at various concentrations in PB (10 mM, pH 7.4) were added. The cells were incubated for 4 h at 37 °C and the cell media was replaced with fresh culture media. Then, the cells were irradiated with NIR laser at an output power of 0.2 W/cm^2 for 10 min. Un-irradiated cells were used as a control. The cells were cultured at 37 °C under an atmosphere containing 5% CO_2 for another 48 h. Then, 20 μL of methyl thiazolyl tetrazolium (MTT, Sigma-Aldrich) solution in PBS (5.0 mg/mL) was added and incubated for another 4 h at 37 °C. The media was aspirated, the MTT-formazan generated by live cells was dissolved in 150 μL of DMSO, and the absorbance at a wavelength of 492 nm of each well was measured using a microplate reader. The relative cell viability (%) was determined by comparing the absorbance at 492 nm with control wells containing only cell culture media. Data are presented as average ± SD (n = 4).

2.7. Confocal microscopy experiment

U87MG cells were plated on microscope slides in a 24-well plate (2×10^5 cells/well) in 500 μL of low glucose Dulbecco's Modified Eagle medium (DMEM) supplemented with 10% fetal bovine serum, 1% L-glutamine, antibiotics penicillin (100 IU/mL), and streptomycin (100 μg/mL) for 12 h. 100 μL of cRGD-HN-DOX, HN-DOX, or free DOX in PBS (10.0 μg DOX/mL) were added. The cells were cultured for 8 h, the media were removed and replenished with fresh cell media, and the cells following 10 min NIR irradiation (0.2 W/cm^2) were cultured for another 5 h. The cells were washed with PBS three times, fixed with 4% formaldehyde for 20 min, and washed with PBS for three times. The cell nuclei were stained with 4′,6-diamidino-2-phenylindole (DAPI, blue) for 20 min. The cells were washed with PBS for three times before confocal fluorescence imaging using a Leica laser scanning confocal microscope. For competitive inhibition experiments, U87MG cells were pretreated for 4 h with free cRGD (10 μmol/L) prior to incubation with cRGD-HN-DOX.

2.8. Blood circulation and in vivo imaging

The mice were handled under protocols approved by Soochow University Laboratory Animal Center. The DOX level in blood was measured by drawing ~10 μL of blood from the tail vein of nude mice at different time points post-injection of cRGD-HN-DOX, HN-DOX, and free DOX (10 mg DOX equiv./kg). Each blood sample was dissolved in 1 mL of lysis buffer (1% SDS, 1% Triton X-100, 40 mM Tris acetate) with brief sonification. DOX was extracted by incubating blood samples in HCl–IPA at −20 °C overnight. After centrifugation at 14.8 krpm for 30 min, the DOX level of the supernatant was determined by fluorescence measurement.

In order to monitor nanoparticles using fluorescence imaging *in vivo*, cRGD-HNs and HNs (non-targeting control) were labeled with Cy7. The human glioma xenograft model was established by subcutaneous inoculation of 5×10^6 U87MG cells in 50 μL serum-free low glucose DMEM medium into the hind flank of each mouse. When the size of tumors reached about 200 mm^3, the tumor-bearing mice were injected with Cy7-labeled cRGD-HNs or HNs, respectively, via tail vein. The fluorescent scans were performed at various time points

(1, 8 and 24 h) post *i.v.* injection using the Maestro *in vivo* fluorescence imaging system (CRi Inc.).

For IR thermal imaging, nude mice bearing U87MG tumors following the treatment with cRGD-HN-DOX, HN-DOX, or PBS were irradiated with 808 nm laser at a power density of 0.1 W/cm^2 for 5 min and simultaneously imaged by an IR thermal camera (Infrared Cameras. Inc.).

2.9. Ex vivo imaging and biodistribution

Taking advantage of the fluorescent nature of DOX, biodistribution studies were also performed *ex vivo* fluorescence imaging. A single dose of cRGD-HN-DOX or HN-DOX in 0.2 mL of PBS was administrated intravenously via the tail vein at a dosage of 10 mg DOX equiv./kg. 8 h later, U87MG tumor-bearing mice administrated with cRGD-HN-DOX or HN-DOX were irradiated with NIR irradiation (808 nm, 0.1 W/cm^2, 5 min). Then, tumor block and several major organs including heart, liver, spleen, lung, and kidney were collected, washed, and dried. Fluorescence images were acquired with the Maestro *in vivo* fluorescence imaging system (CRi Inc.).

To quantify the amount of DOX delivered to the tumor and different organs, tumor-bearing mice following 8 h *i.v.* injection with cRGD-HN-DOX, HN-DOX or free DOX (10 mg DOX equiv./kg) were sacrificed. The tumor block and organs including heart, liver, spleen, lung, and kidney were collected, washed, weighed, and then homogenized in 0.5 mL of lysis buffer (0.25 M sucrose, 10 mM phosphate buffer) with an F6/10 Superfine Homogenizer (Fluko). For DOX measurements, tissue lysate (200 μL) was mixed with Triton X-100 (10%, 100 mL). After strong vortexing, 1.5 mL of the extraction solution (HCl–IPA) was added, and the samples were incubated at −20 °C overnight. After centrifugation at 14.8 krpm for 30 min, the amount of DOX was quantified by fluorescence measurement.

2.10. In vivo antitumor efficacy

U87MG tumor-bearing mice were treated with different DOX formulations including cRGD-HN-DOX with or without irradiation, HN-DOX with irradiation, and free DOX at a dosage of 7.5 mg DOX equiv./kg. The drugs were intravenously injected on a weekly basis. cRGD-HNs with irradiation (without drug) and PBS were used as blank controls. The tumor sizes were measured by calipers twice a week and volume was calculated according to the formula $V = 0.5 \times L \times W^2$, wherein L is the tumor dimension at the longest point and W is the tumor dimension at the widest point. Relative tumor volumes were calculated as V/V_0 (V_0 is the tumor volume when the treatment was initiated). Mice were weighed with the relative body weights normalized to their initial weights. Mice in each cohort were considered to be dead either when the tumor volume increased to 1000 mm^3, or when the mice died during treatment [45].

2.11. Histological analysis

At the end of the treatment, one mouse of each group was sacrificed, and the tumor, liver and kidney were excised. The tissues were fixed with 4% paraformaldehyde solution and embedded in paraffin. The sliced organ tissues (thickness: 4 mm) mounted on the glass slides were stained by hematoxylin and eosin (H&E) and observed by a digital microscope (Leica QWin).

3. Results and discussion

3.1. cRGD-HNs preparation, DOX loading and NIR-triggered drug release

cRGD-directed AuNR/PEG–PCL hybrid nanoparticles (cRGD-HNs) were obtained via capping AuNRs with cRGD-PEG-PCL-LA, which was derived from allyl-PEG-*b*-PCL with an M_n of 7.8–3.0 kg/mol and a low M_w/M_n of 1.06, followed by removing the unconjugated cRGD-PEG-PCL-LA copolymer via centrifugation in water. TEM showed that cRGD-HNs had a monodisperse distribution with a uniform dimension of about 50 nm in length and 15 nm in width (Fig. S1). Thermo gravimetric analysis (TGA) showed that AuNR/PEG-PCL-LA hybrid nanoparticles consisted of ca. 52 *wt.%* of polymer [21]. As expected, cRGD-HNs demonstrated superior stability against extensive dilution to cRGD-PEG-PCL-LA nanoparticles (Fig. S2), due to covalent attachment of PEG-PCL-LA to AuNRs. Furthermore, UV–vis-NIR absorption spectra showed that cRGD-HNs after centrifugation twice had absorptions with transverse and longitudinal plasmonic peaks at ca. 520 nm and 796 nm, similar to CTAB-stabilized AuNRs without centrifugation (Fig. S3), indicating good aqueous stability of cRGD-HNs dispersions. In contrast, no signal was detected for CTAB-stabilized AuNRs following centrifugation twice, confirming better stability of cRGD-HNs than CTAB-stabilized AuNRs. Notably, CTAB is typically used to prepare water dispersible AuNRs. AuNR/PEG-PCL hybrid nanoparticles (HNs) were also prepared via capping AuNRs with PEG–PCL–LA (M_n = 5.0–3.1 kg/mol, M_w/M_n = 1.08) as a non-targeting control [21].

DOX could readily be loaded into cRGD-HNs at pH 7.4 likely through hydrophobic interactions. Excess DOX was removed by extensive dialysis against PB (10 mM, pH 7.4) for 24 h. The results showed that drug loading contents (DLC) increased from 7.46 to 21.7 *wt.%* with increasing theoretical DLC from 10 to 30 *wt.%*, with drug loading efficiencies (DLE) in a range of 64.5–72.6% (Table 1). Dynamic light scattering (DLS) measurements indicated that all DOX-loaded cRGD-HNs (cRGD-HN-DOX) had average hydrodynamic diameters of ca. 90 nm.

The *in vitro* drug release studies showed that DOX release from cRGD-HN-DOX was minimal without NIR irradiation (less than 10% in 4 h) (Fig. 1), supporting that cRGD-HN-DOX is robust and premature drug release is effectively inhibited. Notably, DOX release from cRGD-HN-DOX was markedly boosted, e.g. from 2.0% to 32.6% at 1 h, upon 5 min irradiation with an 808 nm NIR laser at a mild power density of 0.2 W/cm^2. The drug release was practically turned off following retreating NIR irradiation. NIR-triggered drug release was observed when the same laser treatment (0.2 W/cm^2, 5 min) was repeated at 2 h, 3 h, and 4 h, in which drug release was augmented from 33.5% to 53.7%, from 54.5% to 66.6%, and from 67.9% to 75.4%, respectively (Fig. 1). It is evident, therefore, that DOX release from cRGD-HN-DOX could be well-controlled by NIR laser, similar to our previous report [21].

3.2. Antitumor activity of cRGD-HN-DOX toward U87MG cells

The *in vitro* antitumor activity of cRGD-HN-DOX was evaluated by MTT assays in $\alpha_v\beta_3$ integrin receptor over-expressed glioblastoma U87MG cells. The cells were incubated with cRGD-HN-DOX, HN-DOX, cRGD-HNs, HNs or free DOX (5.0 and 10 μg DOX equiv./mL) for 4 h at 37 °C, the media were removed and replenished with fresh culture media, and the cells following 10 min irradiation with NIR laser (808 nm, 0.2 W/cm^2) were cultured for another 48 h. MTT assays showed that both cRGD-HNs and HNs, either with or without NIR irradiation were practically non-toxic (cell viabilities

Table 1
Loading of DOX into cRGD-HNs. Data are presented as mean ± SD (n = 3).

Entry	DLC (*wt.%*)[a]		DLE (%)[a]	Size (nm)[b]
	Theory	Determined		
1	10	7.46 ± 0.4	72.6 ± 1.3	90 ± 2
2	20	14.4 ± 0.6	67.4 ± 1.8	94 ± 2
3	30	21.7 ± 0.5	64.5 ± 2.2	89 ± 1

[a] Drug loading content (DLC) and drug loading efficiency (DLE) determined by fluorescence measurement.
[b] Determined by DLS.

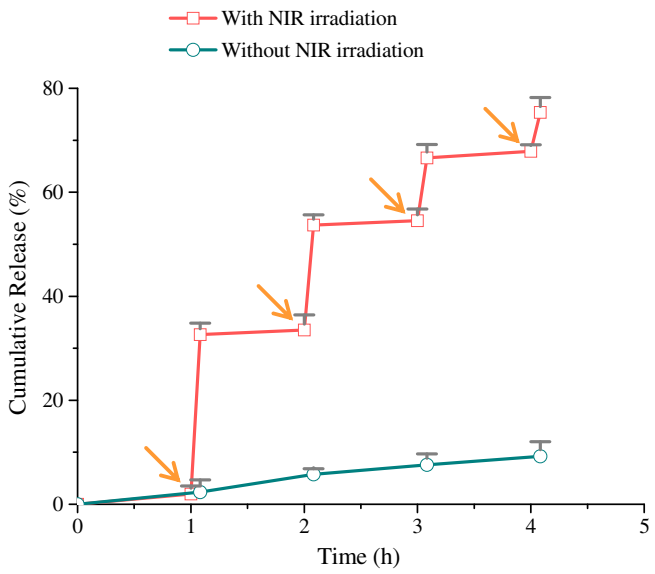

Fig. 1. NIR-triggered DOX release at pH 7.4. cRGD-HN-DOX dispersions were irradiated with NIR laser (808 nm, 0.2 W/cm^2) for 5 min at 1, 2, 3, and 4 h.

>96.3%) (Fig. 2A), indicating that cRGD-HNs and HNs possess excellent biocompatibility, and such mild NIR irradiation has little adverse effect to cells. Interestingly, cRGD-HN-DOX and HN-DOX exhibited low antitumor effect even at 10 μg DOX equiv./mL (cell viabilities >85.2%), which is in accordance with their inhibited drug release (Fig. 1). However, markedly enhanced antitumor activity was achieved for cRGD-HN-DOX with 10 min NIR irradiation under otherwise the same conditions, wherein low cell viabilities of 58.2% and 30.0% were observed at 5.0 and 10 μg DOX equiv./mL, respectively (Fig. 2A). The antitumor activity of non-targeting HN-DOX was also enhanced by NIR irradiation (80.9% and 72.7% cell viabilities at 5.0 and 10 μg DOX equiv./mL, respectively), though far lower than cRGD-HN-DOX. In contrast, such NIR irradiation caused little effect to U87MG cells treated with free DOX. It should further be noted that cRGD-HN-DOX with 10 min NIR irradiation exhibited significantly higher antitumor activity in U87MG cells than free DOX at a dosage of 10 μg DOX equiv./mL (cell viabilities 30.0% *versus* 42.3%). These results support that cRGD-HN-DOX possess apparent targetability to U87MG cells and drug release from cRGD-HN-DOX inside the cells is greatly enhanced by NIR irradiation. Further studies showed that cRGD-HN-DOX with NIR irradiation had IC_{50} (half maximal inhibitory concentration) of 6.2 μg DOX/mL, which was ca. 8 times lower than non-targeting HN-DOX under otherwise the same conditions (IC_{50} = 50.8 μg DOX/mL) and comparable to free DOX (IC_{50} = 5.7 μg/mL) (Fig. 2B).

The cellular uptake and intracellular drug release behaviors of cRGD-HN-DOX were studied in U87MG cells using confocal microscopy. Here, U87MG cells were incubated with cRGD-HN-DOX and HN-DOX (10 μg DOX equiv./mL) for 8 h at 37 °C, the media were removed and replenished with fresh culture media, the cells following 10 min irradiation with NIR laser (808 nm, 0.2 W/cm^2) were cultured for another 5 h. The results showed strong DOX fluorescence in the nuclei of U87MG cells treated with cRGD-HN-DOX, which was significantly higher than that with HN-DOX (non-targeting control) under otherwise the same conditions and comparable to that with free DOX (Fig. S4), indicating that cRGD-HN-DOX is taken up by U87MG cells via a receptor-mediated mechanism and DOX is efficiently released by NIR irradiation. In contrast, U87MG cells treated with cRGD-HN-DOX but without NIR irradiation displayed only negligible DOX fluorescence. The competitive inhibition experiments showed that minimal DOX fluorescence was observed in U87MG cells pretreated with free cRGD prior to incubation with cRGD-HN-DOX (with NIR irradiation), conforming active targeting effect of cRGD-HN-DOX toward U87MG cells. These confocal microscopy observations are consistent with the *in vitro* antitumor activity results by MTT assays.

3.3. In vivo pharmacokinetics and imaging studies

In the following, we investigated the *in vivo* pharmacokinetics of cRGD-HN-DOX in mice. The plasma levels of DOX were determined by fluorescence spectroscopy at different time intervals following a single *i.v.* injection of cRGD-HN-DOX, HN-DOX, or free DOX (10 mg

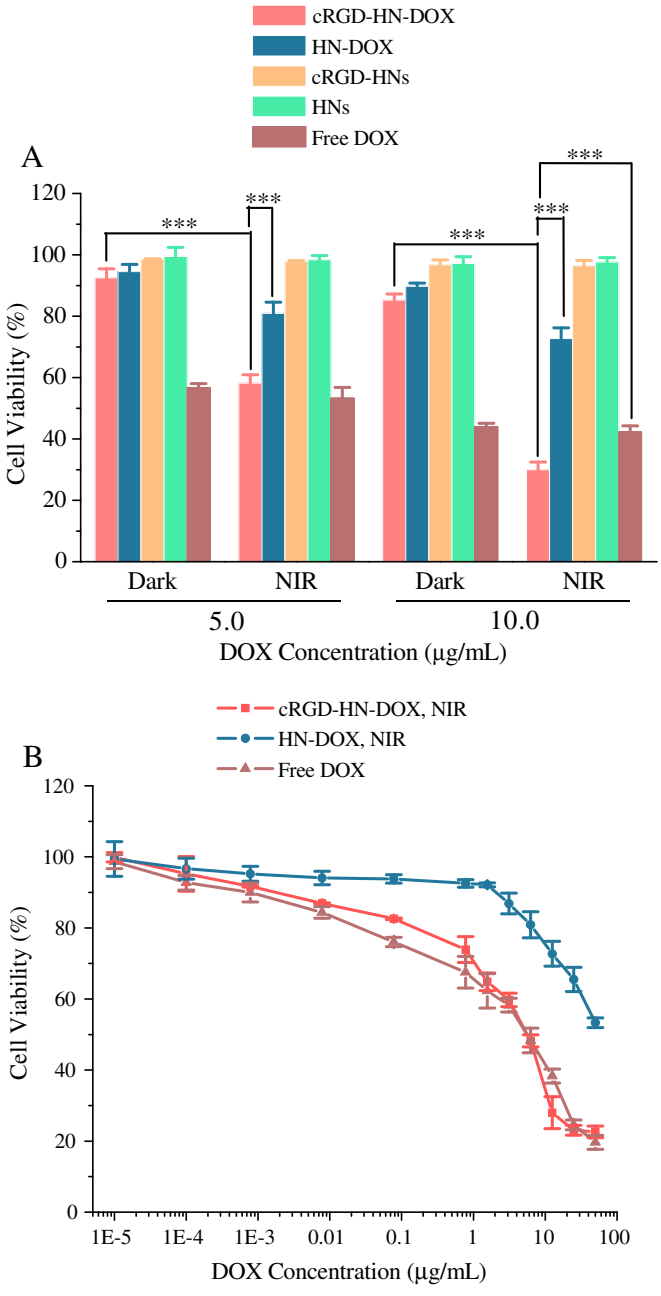

Fig. 2. MTT assays. (A) Cytotoxicity of HN-DOX, cRGD-HNs, HNs, and free DOX in U87MG cells. The cells were incubated with cRGD-HN-DOX, HN-DOX, cRGD-HNs, HNs or free DOX (5.0 and 10 μg DOX equiv./mL) for 4 h at 37 °C, the media were removed and replenished with fresh culture media, the cells following 10 min irradiation with NIR laser (808 nm, 0.2 W/cm^2) were cultured for another 48 h before MTT assays; and (B) Dependence of U87MG cell viabilities on DOX concentrations. The cells were treated by cRGD-HN-DOX with NIR irradiation, HN-DOX with NIR irradiation, and free DOX, respectively. Data are shown as mean ± SD (n = 4). *p < 0.05, **p < 0.01, and ***p < 0.001 (Student's *t* test).

DOX equiv./kg) in nude mice. Notably, cRGD-HN-DOX and HN-DOX revealed a significantly longer circulation time than free DOX, in which the concentration of DOX in plasma decreased to undetectable levels after 2 h injection of free DOX, whereas considerable amount of DOX was observed even at 24 h following administration of cRGD-HN-DOX and HN-DOX (Fig. 3A). The long circulation time in blood might be attributed to the efficient PEG shielding as well as high stability of hybrid nanoparticles. The distribution phase half-lives were determined to be 0.53, 0.37, and 0.28 h, while the elimination phase half-lives were 5.95, 4.94, and 0.30 h, for cRGD-HN-DOX, HN-DOX and free DOX, respectively. The slightly longer circulation time of cRGD-HN-DOX as compared to HN-DOX is most likely due to their relatively longer PEG chain (M_n of PEG: 7.8 kg/mol for cRGD-HN-DOX *versus* 5.0 kg/mol for HN-DOX), as shown by previous reports [46,47].

To evaluate their *in vivo* tumor-targetability, Cy7-labeled cRGD-HNs or Cy7-labeled HNs were injected intravenously to mice bearing human U87MG tumor xenografts and monitored using a Maestro EX *in vivo* fluorescence imaging system (CRi, Inc.). The fluorescence images showed significant tumor accumulation of cRGD-HNs at 1 h post injection and strong fluorescence in the tumor site at 8 h and even 24 h post injection (Fig. 3B), confirming high tumor accumulation and retention of cRGD-HNs. In comparison, Cy7-labeled HNs (non-targeting control) exhibited significantly less tumor accumulation (Fig. 3B), though cRGD-HNs and HNs had similar circulation time. These results indicate that targeting ligands like cRGD play an important role in achieving high tumor accumulation and retention [38,48,49].

An IR thermal camera was used to monitor the temperature changes on mice during laser irradiation. In the following *in vivo* experiments, we adopted a lower laser output power density of 0.1 W/cm^2 to prevent marked increase of temperature in the tumor tissue which could lead to

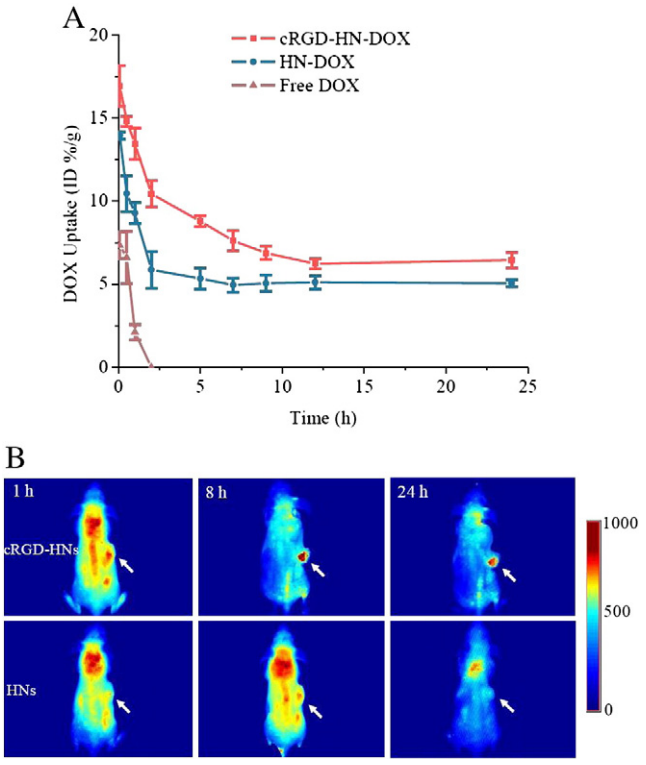

Fig. 3. *In vivo* pharmacokinetics and imaging studies. (A) *In vivo* pharmacokinetics of cRGD-HN-DOX, HN-DOX and free DOX in mice. DOX levels were determined by fluorescence spectroscopy. DOX uptake is expressed as injected dose per gram of tissue (%ID/g). Data are presented as mean ± SD (n = 3); and (B) *in vivo* fluorescence images of U87MG tumor-bearing nude mice at different time points following injection of Cy7-labeled cRGD-HNs or HNs. The mouse autofluorescence was removed by spectral unmixing using the Maestro software.

photothermal ablation of tumor. The results showed that NIR laser irradiation (808 nm, 0.1 W/cm^2, 5 min) at 2, 8 and 24 h following *i.v.* injection of cRGD-HN-DOX led to localized heating in the tumor region, where tumor temperature was much increased but not exceeding 45 °C (Fig. 4). The highest tumor temperature was observed at 8 h post-injection, which was consistent with the *in vivo* fluorescence imaging results. In contrast, mice injected with non-targeting HN-DOX showed only a moderate tumor temperature increase, and those injected with PBS exhibited no obvious increase of tumor temperature under otherwise the same conditions (Fig. 4). These observations have further confirmed that cRGD-HN-DOX can effectively target to and accumulate in the glioma xenografts in mice.

3.4. Ex vivo fluorescence imaging and biodistribution

To examine the distribution of released DOX in tumor-bearing mice, ex vivo fluorescence images of tumor and several major organs following 8 h *i.v.* injection of cRGD-HN-DOX or HN-DOX and NIR irradiation were taken. As the fluorescence of DOX encapsulated in the nanoparticles is self-quenched, detected fluorescence is due to free DOX [29,50]. The *ex vivo* fluorescence images revealed that mice treated with cRGD-HN-DOX had strong DOX fluorescence in the tumor, which was significantly stronger than that in the major organs such as heart, liver, spleen, lung and kidney (Fig. 5A). In comparison, non-targeting HN-DOX exhibited weak DOX fluorescence in the tumor while strong DOX fluorescence in the liver, lung and kidney. These results signify that cRGD-HN-DOX can effectively target to human glioma xenografts and drug release *in vivo* can be triggered by NIR irradiation. In the following, the amount of DOX accumulated in tumors and major organs such as spleen, liver, kidney, heart and lung were quantified using fluorescence measurement. The tumor uptake of DOX was 4.06% of injected dose per gram of tissue (%ID/g) for cRGD-HN-DOX, which was over 3-fold higher than that for HN-DOX (1.24%ID/g) (Fig. 5B). Moreover, cRGD-HN-DOX displayed reduced accumulation in lung, liver, spleen, and kidney as compared with HN-DOX. The tumor-to-normal tissue (T/N) distribution ratios of DOX are summarized in Table 2. These collected data demonstrated that cRGD-HN-DOX upon irradiation could in general reduce DOX uptake by healthy organs or tissues particularly lung, liver, spleen and kidney while largely increase DOX accumulation in the glioblastoma tumors.

The therapeutic performance of cRGD-HN-DOX in combination with NIR irradiation was evaluated using U87MG tumor-bearing nude mice. When tumors grew up to about 30 mm^3 in volume, mice were treated with cRGD-HN-DOX and HN-DOX (7.5 mg DOX equiv./kg) and irradiated with NIR laser (808 nm, 0.1 W/cm^2, 5 min) at 8 h post injection. The treatment was repeated once a week, cRGD-HN-DOX without NIR irradiation, cRGD-HNs with NIR irradiation, free DOX and PBS were used as controls. The results showed that mice treated with cRGD-HN-DOX and NIR irradiation completely inhibited tumor growth, which was significantly more effective than non-targeting HN-DOX under otherwise the same conditions (relative tumor volume at day 24: 0.98 *versus* 5.26) (Fig. 6A). In contrast, cRGD-HN-DOX without NIR irradiation exhibited low antitumor effect (relative tumor volume = 10.94). It should further be noted cRGD-HNs with NIR irradiation had little inhibition of tumor growth. These results signify the importance of cRGD targeting and NIR triggered drug release for effective tumor inhibition. Notably, free DOX treatment could also slow down tumor growth but not so effective as cRGD-HN-DOX with NIR irradiation (relative tumor volume: 0.98 *versus* 1.92). The photographs of tumor blocks isolated at day 25 confirmed that mice treated with cRGD-HN-DOX in combination with NIR irradiation had the smallest tumor size (Fig. 6B). Importantly, mice treated with cRGD-HN-DOX had little change of body weights, which was in sharp contrast to ca. 34% body weight loss for mice treated with free DOX (Fig. 6C), indicating that cRGD-HN-DOX has little systemic toxicity. Remarkably, Kaplan–Meier survival curve showed that mice treated with cRGD-HN-DOX in

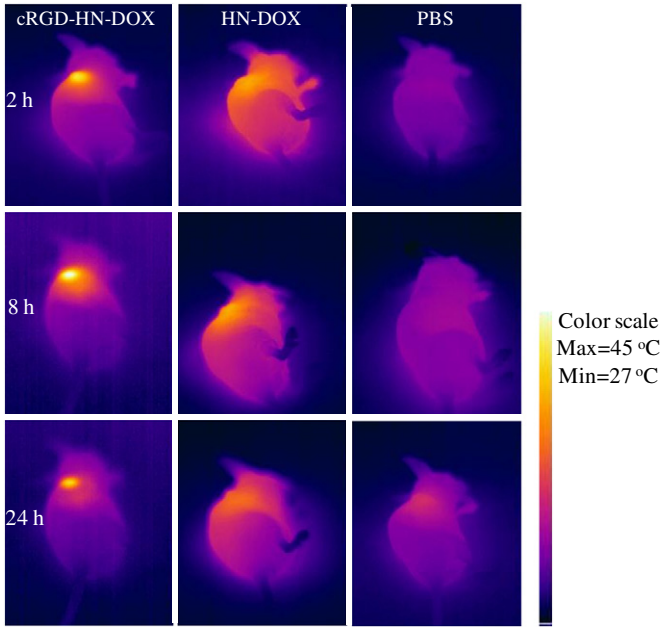

Fig. 4. IR thermal images of tumor-bearing mice exposed to the NIR laser (808 nm, 0.1 W/cm^2, 5 min) at 2, 8 and 24 h after *i.v.* injection with cRGD-HN-DOX, HN-DOX and PBS, respectively.

combination with NIR irradiation all survived over an experimental period of 48 days without a single death (Fig. 6D). Improved survival rate was also observed for mice treated with cRGD-HNs plus NIR irradiation. In contrast, little improvement on survival time was observed for mice treated with cRGD-HN-DOX without NIR irradiation

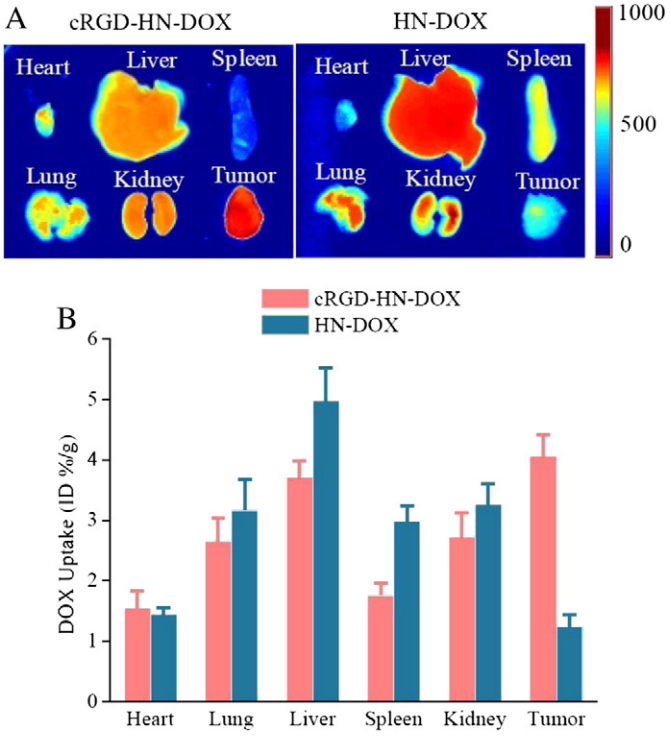

Fig. 5. *In vivo* biodistribution of cRGD-HN-DOX and HN-DOX in U87MG glioma bearing nude mice following 8 h intravenous injection and NIR irradiation (808 nm, 0.1 W/cm^2, 5 min). (A) DOX fluorescence images of tumors and organs; and (B) quantification of DOX accumulated in different organs and tumors using fluorescence spectroscopy. DOX uptake is expressed as injected dose per gram of tissue (%ID/g). Data are presented as mean ± SD (n = 3).

Table 2
Summary of tumor-to-normal tissue (T/N) distribution ratios of DOX at 8 h after *i.v.* injection and NIR irradiation. Data are presented as mean ± SD (n = 3).

	Heart	Lung	Liver	Spleen	Kidney
cRGD-HN-DOX	2.62 ± 0.21	1.53 ± 0.05	1.09 ± 0.51	2.31 ± 0.82	1.49 ± 0.27
HN-DOX	0.86 ± 0.10	0.31 ± 0.02	0.25 ± 0.05	0.42 ± 0.13	0.38 ± 0.06

as well as free DOX. The histological analysis using H&E staining revealed that tumor tissues of mice treated with cRGD-HN-DOX plus NIR irradiation underwent significantly more extensive necrosis than those treated with non-targeting HN-DOX plus NIR irradiation and free DOX (Fig. 7). Moreover, cRGD-HN-DOX and HN-DOX with NIR irradiation induced little damage to liver and kidney while significant liver necrosis was observed for mice treated with free DOX. These combined results demonstrate that cRGD-directed and NIR-sensitive AuNR/PEG–PCL hybrid nanoparticles can not only significantly enhance therapeutic efficacy of DOX but also markedly decrease its side effects.

This study provides a proof of concept that cRGD-HN-DOX can accumulate and efficiently release drugs into a subcutaneous solid tumor model by mild NIR irradiation, leading to effective inhibition of tumor growth. It should be noted that for brain tumor, poor drug penetration from vessels into tumors caused by the vascular/tumor barrier such as blood–brain barrier (BBB) and blood–brain tumor barrier (BBTB), results in low therapeutic efficacy. The presence of cRGD ligand in cRGD-HN-DOX might facilitate the translocation of drug carriers across the endothelium of the tumor vasculature as well as selective uptake by glioblastoma cells [37,51]. Moreover, NIR laser would trigger drug release from cRGD-HN-DOX nanoparticles accumulated in the tumor vasculature and extracellular milieu, which might also enhance drug tumor penetration. In the following, we will study the distribution, accumulation and therapeutic performances of cRGD-HN-DOX in the orthotopic glioma models.

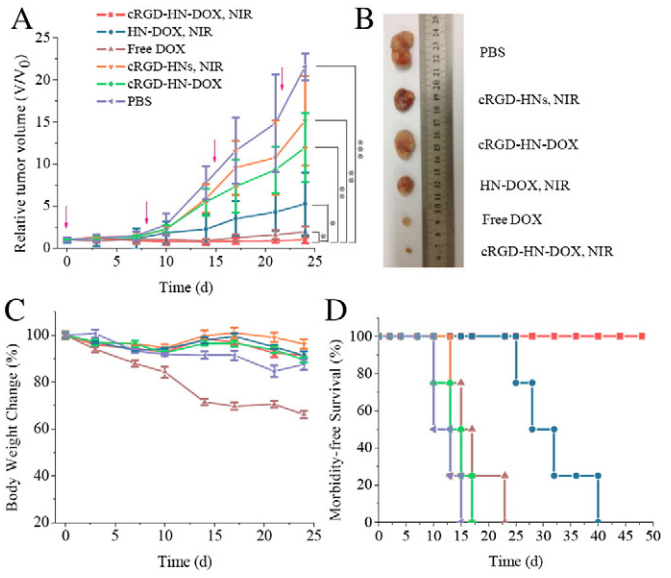

Fig. 6. *In vivo* antitumor performance of cRGD-HN-DOX with NIR irradiation. (A) Tumor volume changes of U87MG tumor-bearing nude mice treated with cRGD-HN-DOX plus NIR irradiation (808 nm, 0.1 W/cm^2, 5 min) at 8 h post-injection. The drug was given on day 0, 8, 15, and 22 (dosage: 7.5 mg DOX equiv./kg body weight, in 0.2 mL PBS). Mice treated with HN-DOX plus NIR irradiation, free DOX, cRGD-HN plus NIR irradiation, cRGD-HN-DOX, and PBS were used as controls. Data are presented as mean ± SD (n = 6). *$p < 0.05$, **$p < 0.01$, and ***$p < 0.001$ (Student's *t* test); (B) photographs of tumor blocks collected from different treatment groups of mice on day 25; (C) body weight changes of mice in different treatment groups within 24 d. Data are presented as mean ± SD (n = 6); and (D) survival rates of mice in different treatment groups within 48 d.

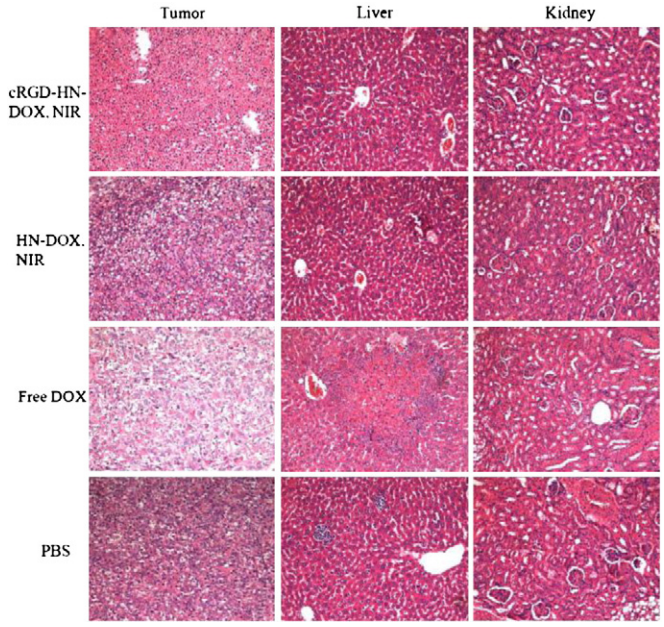

Fig. 7. H&E-stained tumor, liver and kidney sections excised from U87MG tumor-bearing mice following 25 day treatment with cRGD-HN-DOX plus NIR irradiation. Mice treated with HN-DOX plus NIR irradiation, free DOX, and PBS were used as controls. The images were obtained under a Leica microscope using a 20× objective.

4. Conclusions

We have demonstrated for the first time that cRGD-functionalized and NIR-responsive AuNR/PEG–PCL hybrid nanoparticles mediate targeted delivery as well as remotely controlled release of doxorubicin into human glioblastoma xenografts in mice, leading to complete inhibition of tumor growth with little adverse effects and 100% mice survival over an experimental period of 48 days. These hybrid nanoparticles have appeared as an innovative and promising platform for targeted cancer chemotherapy *in vivo* in that (i) they have excellent colloidal stability, inhibited drug leakage, and prolonged blood circulation time; (ii) they display greatly enhanced accumulation and retention in the glioblastoma as compared to the non-targeting counterparts; (iii) they are efficiently internalized by glioblastoma cells via the receptor-mediated endocytosis mechanism; (iv) remarkably, they allow precise temporal as well as spatial control over drug release rate and dosage via mild NIR irradiation *in vivo*; and (v) they are biocompatible and easy to prepare with well-defined structure and size. It should further be noted that the hybrid nanoparticle systems are highly versatile and can be applied for the delivery of various hydrophobic drugs and treatment of different malignant tumors using a selected type of ligands.

Acknowledgments

This work is financially supported by research grants from the National Natural Science Foundation of China (NSFC 51173126, 51273139, 51103093, 51273137, 51003070 and 81261120557), the National Science Fund for Distinguished Young Scholars (NSFC 51225302), Jiangsu Specially-Appointed Professorship, Ph.D. Programs Foundation of Ministry of Education of China (20133201110005), a project funded by the Priority Academic Program Development of Jiangsu Higher Education Institutions (PAPD 233200613). Innovative Graduate Research Program of Jiangsu Province (CXZZ13_0805).

Appendix A. Supplementary data

Supplementary data to this article can be found online at http://dx.doi.org/10.1016/j.jconrel.2014.07.054.

References

[1] N. Wiradharma, Y. Zhang, S. Venkataraman, J.L. Hedrick, Y.Y. Yang, Self-assembled polymer nanostructures for delivery of anticancer therapeutics, Nano Today 4 (2009) 302–317.
[2] J. Nicolas, S. Mura, D. Brambilla, N. Mackiewicz, P. Couvreur, Design, functionalization strategies and biomedical applications of targeted biodegradable/biocompatible polymer-based nanocarriers for drug delivery, Chem. Soc. Rev. 42 (2013) 1147–1235.
[3] M. Elsabahy, K.L. Wooley, Design of polymeric nanoparticles for biomedical delivery applications, Chem. Soc. Rev. 41 (2012) 2545–2561.
[4] T.-Y. Kim, D.-W. Kim, J.-Y. Chung, S.G. Shin, S.-C. Kim, D.S. Heo, N.K. Kim, Y.-J. Bang, Phase I and pharmacokinetic study of Genexol-PM, a cremophor-free, polymeric micelle-formulated paclitaxel, in patients with advanced malignancies, Clin. Cancer Res. 10 (2004) 3708–3716.
[5] J. Hrkach, D. Von Hoff, M.M. Ali, E. Andrianova, J. Auer, T. Campbell, D. De Witt, M. Figa, M. Figueiredo, A. Horhota, Preclinical development and clinical translation of a PSMA-targeted docetaxel nanoparticle with a differentiated pharmacological profile, Sci. Transl. Med. 4 (2012) 128ra139.
[6] Y.H. Bae, H. Yin, Stability issues of polymeric micelles, J. Control. Release 131 (2008) 2–4.
[7] C. Deng, Y.J. Jiang, R. Cheng, F.H. Meng, Z.Y. Zhong, Biodegradable polymeric micelles for targeted and controlled anticancer drug delivery: promises, progress and prospects, Nano Today 7 (2012) 467–480.
[8] T. Lammers, F. Kiessling, W.E. Hennink, G. Storm, Drug targeting to tumors: principles, pitfalls and (pre-) clinical progress, J. Control. Release 161 (2012) 175–187.
[9] R.K. O'Reilly, C.J. Hawker, K.L. Wooley, Cross-linked block copolymer micelles: functional nanostructures of great potential and versatility, Chem. Soc. Rev. 35 (2006) 1068–1083.
[10] F. Meng, R. Cheng, C. Deng, Z. Zhong, Intracellular drug release nanosystems, Mater. Today 15 (2012) 436–442.
[11] A.N. Koo, H.J. Lee, S.E. Kim, J.H. Chang, C. Park, C. Kim, J.H. Park, S.C. Lee, Disulfide-cross-linked PEG-poly (amino acid)s copolymer micelles for glutathione-mediated intracellular drug delivery, Chem. Commun. (2008) 6570–6572.
[12] Y. Wu, W. Chen, F. Meng, Z. Wang, R. Cheng, C. Deng, H. Liu, Z. Zhong, Core-crosslinked pH-sensitive degradable micelles: a promising approach to resolve the extracellular stability *versus* intracellular drug release dilemma, J. Control. Release 164 (2012) 338–345.
[13] S.J. Lee, K.H. Min, H.J. Lee, A.N. Koo, H.P. Rim, B.J. Jeon, S.Y. Jeong, J.S. Heo, S.C. Lee, Ketal cross-linked poly(ethylene glycol)–poly(amino acid)s copolymer micelles for efficient intracellular delivery of doxorubicin, Biomacromolecules 12 (2011) 1224–1233.
[14] M. Talelli, M. Iman, A.K. Varkouhi, C.J. Rijcken, R.M. Schiffelers, T. Etrych, K. Ulbrich, C.F. van Nostrum, T. Lammers, G. Storm, Core-crosslinked polymeric micelles with controlled release of covalently entrapped doxorubicin, Biomaterials 31 (2010) 7797–7804.
[15] F. Meng, Y. Zhong, R. Cheng, C. Deng, Z. Zhong, pH-sensitive polymeric nanoparticles for tumor-targeting doxorubicin delivery: concept and recent advances, Nanomedicine 9 (2014) 487–499.
[16] A.N. Koo, K.H. Min, H.J. Lee, S.-U. Lee, K. Kim, I. Chan Kwon, S.H. Cho, S.Y. Jeong, S.C. Lee, Tumor accumulation and antitumor efficacy of docetaxel-loaded core-shell-corona micelles with shell-specific redox-responsive cross-links, Biomaterials 33 (2012) 1489–1499.
[17] J. Dai, S. Lin, D. Cheng, S. Zou, X. Shuai, Interlayer-crosslinked micelle with partially hydrated core showing reduction and pH dual sensitivity for pinpointed intracellular drug release, Angew. Chem. Int. Ed. 50 (2011) 9404–9408.
[18] S.-Y. Lee, S. Kim, J.Y. Tyler, K. Park, J.-X. Cheng, Blood-stable, tumor-adaptable disulfide bonded mPEG-$(Cys)_4$-PDLLA micelles for chemotherapy, Biomaterials 34 (2013) 552–561.
[19] Y. Li, K. Xiao, J. Luo, W. Xiao, J.S. Lee, A.M. Gonik, J. Kato, T.A. Dong, K.S. Lam, Well-defined, reversible disulfide cross-linked micelles for on-demand paclitaxel delivery, Biomaterials 32 (2011) 6633–6645.
[20] S. Yu, J. Ding, C. He, Y. Cao, W. Xu, X. Chen, Disulfide cross-linked polyurethane micelles as a reduction-triggered drug delivery system for cancer therapy, Adv. Healthc. Mater. 3 (2013) 752–760.
[21] Y. Zhong, C. Wang, L. Cheng, F. Meng, Z. Zhong, Z. Liu, Gold nanorod-cored biodegradable micelles as a robust and remotely controllable doxorubicin release system for potent inhibition of drug-sensitive and-resistant cancer cells, Biomacromolecules 14 (2013) 2411–2419.
[22] J. Liu, C. Detrembleur, B. Grignard, D. Pauw-Gillet, S. Mornet, M. Treguer-Delapierre, Y. Petit, C. Jérôme, E. Duguet, Gold nanorods with phase-changing polymer corona for remotely near-infrared-triggered drug release, Chem. Asian. J. 9 (2014) 275–288.
[23] U. Singh, I. Jialal, Retracted: alpha-lipoic acid supplementation and diabetes, Nutr. Rev. 66 (2008) 646–657.
[24] A. Maczurek, K. Hager, M. Kenklies, M. Sharman, R. Martins, J. Engel, D.A. Carlson, G. Münch, Lipoic acid as an anti-inflammatory and neuroprotective treatment for Alzheimer's disease, Adv. Drug Delivery Rev. 60 (2008) 1463–1470.
[25] J. Sharma, R. Chhabra, C.S. Andersen, K.V. Gothelf, H. Yan, Y. Liu, Toward reliable gold nanoparticle patterning on self-assembled DNA nanoscaffold, J. Am. Chem. Soc. 130 (2008) 7820–7821.
[26] J. van Herrikhuyzen, S.J. George, M.R. Vos, N.A. Sommerdijk, A. Ajayaghosh, S.C. Meskers, A.P. Schenning, Self-assembled hybrid oligo (p-phenylenevinylene)-gold nanoparticle tapes, Angew. Chem. Int. Ed. 46 (2007) 1825–1828.
[27] A.A. Volkert, V. Subramaniam, M.R. Ivanov, A.M. Goodman, A.J. Haes, Salt-mediated self-assembly of thioctic acid on gold nanoparticles, ACS Nano 5 (2011) 4570–4580.

[28] G. Zhang, Z. Yang, W. Lu, R. Zhang, Q. Huang, M. Tian, L. Li, D. Liang, C. Li, Influence of anchoring ligands and particle size on the colloidal stability and *in vivo* biodistribution of polyethylene glycol-coated gold nanoparticles in tumor-xenografted mice, Biomaterials 30 (2009) 1928–1936.
[29] Y.L. Li, L. Zhu, Z. Liu, R. Cheng, F. Meng, J.H. Cui, S.J. Ji, Z. Zhong, Reversibly stabilized multifunctional dextran nanoparticles efficiently deliver doxorubicin into the nuclei of cancer cells, Angew. Chem. Int. Ed. 48 (2009) 9914–9918.
[30] L. Wu, Y. Zou, C. Deng, R. Cheng, F. Meng, Z. Zhong, Intracellular release of doxorubicin from core-crosslinked polypeptide micelles triggered by both pH and reduction conditions, Biomaterials 34 (2013) 5262–5272.
[31] R. Wei, L. Cheng, M. Zheng, R. Cheng, F. Meng, C. Deng, Z. Zhong, Reduction-responsive disassemblable core-cross-linked micelles based on poly (ethylene glycol)-b-poly (N-2-hydroxypropyl methacrylamide)–lipoic acid conjugates for triggered intracellular anticancer drug release, Biomacromolecules 13 (2012) 2429–2438.
[32] Y. Xu, F. Meng, R. Cheng, Z. Zhong, Reduction-sensitive reversibly crosslinked biodegradable micelles for triggered release of doxorubicin, Macromol. Biosci. 9 (2009) 1254–1261.
[33] M. Zheng, Y. Zhong, F. Meng, R. Peng, Z. Zhong, Lipoic acid modified low molecular weight polyethylenimine mediates nontoxic and highly potent *in vitro* gene transfection, Mol. Pharmaceutics 8 (2011) 2434–2443.
[34] J.S. Desgrosellier, D.A. Cheresh, Integrins in cancer: biological implications and therapeutic opportunities, Nat. Rev. Cancer 10 (2010) 9–22.
[35] Y. Zhong, F. Meng, C. Deng, Z. Zhong, Ligand-directed active tumor-targeting polymeric nanoparticles for cancer chemotherapy, Biomacromolecules 15 (2014) 1955–1969.
[36] Y. Miura, T. Takenaka, K. Toh, S. Wu, H. Nishihara, M.R. Kano, Y. Ino, T. Nomoto, Y. Matsumoto, H. Koyama, Cyclic RGD-linked polymeric micelles for targeted delivery of platinum anticancer drugs to glioblastoma through the blood–brain tumor barrier, ACS Nano 7 (2013) 8583–8592.
[37] C. Zhan, B. Gu, C. Xie, J. Li, Y. Liu, W. Lu, Cyclic RGD conjugated poly (ethylene glycol)-*co*-poly (lactic acid) micelle enhances paclitaxel anti-glioblastoma effect, J. Control. Release 143 (2010) 136–142.
[38] C. Zhan, X. Wei, J. Qian, L. Feng, J. Zhu, W. Lu, Co-delivery of TRAIL gene enhances the anti-glioblastoma effect of paclitaxel *in vitro* and *in vivo*, J. Control. Release 160 (2012) 630–636.
[39] C.L. Waite, C.M. Roth, PAMAM–RGD conjugates enhance siRNA delivery through a multicellular spheroid model of malignant glioma, Bioconjugate Chem. 20 (2009) 1908–1916.
[40] R. Yang, F. Meng, S. Ma, F. Huang, H. Liu, Z. Zhong, Galactose-decorated cross-linked biodegradable poly (ethylene glycol)-b-poly (ε-caprolactone) block copolymer micelles for enhanced hepatoma-targeting delivery of paclitaxel, Biomacromolecules 12 (2011) 3047–3055.
[41] J. Stefely, M.A. Markowitz, S.L. Regen, Permeability characteristics of lipid bilayers from lipoic acid-derived phosphatidylcholines: comparison of monomeric, crosslinked and noncrosslinked polymerized membranes, J. Am. Chem. Soc. 110 (1988) 7463–7469.
[42] T.K. Sau, C.J. Murphy, Seeded high yield synthesis of short Au nanorods in aqueous solution, Langmuir 20 (2004) 6414–6420.
[43] H. Liao, J.H. Hafner, Gold nanorod bioconjugates, Chem. Mater. 17 (2005) 4636–4641.
[44] K.M. Laginha, S. Verwoert, G.J.R. Charrois, T.M. Allen, Determination of doxorubicin levels in whole tumor and tumor nuclei in murine breast cancer tumors, Clin. Cancer Res. 11 (2005) 6944–6949.
[45] L. Cheng, K. Yang, Y. Li, X. Zeng, M. Shao, S.-T. Lee, Z. Liu, Multifunctional nanoparticles for upconversion luminescence/MR multimodal imaging and magnetically targeted photothermal therapy, Biomaterials 33 (2012) 2215–2222.
[46] D.E. Owens III, N.A. Peppas, Opsonization, biodistribution, and pharmacokinetics of polymeric nanoparticles, Int. J. Pharmaceut. 307 (2006) 93–102.
[47] R. Gref, A. Domb, P. Quellec, T. Blunk, R. Müller, J. Verbavatz, R. Langer, The controlled intravenous delivery of drugs using PEG-coated sterically stabilized nanospheres, Adv. Drug Delivery Rev. 16 (1995) 215–233.
[48] P. Liu, L. Qin, Q. Wang, Y. Sun, M. Zhu, M. Shen, Y. Duan, cRGD-functionalized mPEG-PLGA-PLL nanoparticles for imaging and therapy of breast cancer, Biomaterials 33 (2012) 6739–6747.
[49] N. Yonenaga, E. Kenjo, T. Asai, A. Tsuruta, K. Shimizu, T. Dewa, M. Nango, N. Oku, RGD-based active targeting of novel polycation liposomes bearing siRNA for cancer treatment, J. Control. Release 160 (2012) 177–181.
[50] Y. Bae, S. Fukushima, A. Harada, K. Kataoka, Design of environment-sensitive supramolecular assemblies for intracellular drug delivery: polymeric micelles that are responsive to intracellular pH change, Angew. Chem. Int. Ed. 42 (2003) 4640–4643.
[51] J. Choi, J. Yang, J. Park, E. Kim, J.S. Suh, Y.M. Huh, S. Haam, Specific near-IR absorptionimaging of glioblastomas using integrin-targeting gold nanorods, Adv. Funct. Mater. 21 (2011) 1082–1088.